



Contents lists available at ScienceDirect

Defence Technology

journal homepage: www.elsevier.com/locate/dt

Bore-center annular shaped charges with different liner materials penetrating into steel targets

Wen-long Xu ^a, Cheng Wang ^{a,*}, Jian-ming Yuan ^b, Tao Deng ^a

^a State Key Lab of Explosion Science and Technology, Beijing Institute of Technology, Beijing, 100081, China

^b Temasek Laboratories, Nanyang Technological University, 50 Nanyang Drive, 637553, Singapore

ARTICLE INFO

Article history:

Received 28 February 2019

Received in revised form

24 May 2019

Accepted 1 July 2019

Available online xxx

Keywords:

Annular shaped charge

Liner material

Formation

Numerical simulation

ABSTRACT

The bore-center annular shaped charge (BCASC) is a new type of shaped charge which can generate a larger-diameter hole in steel targets than classical shaped charges. In this paper, the influence of three liner materials, i.e. molybdenum, nickel and copper, on BCASC formation and penetrating into steel targets was investigated by experiment and numerical simulation. The simulation results were well consistent with the experimental results. This study showed that, at $0.50D$ standoff distance, the axial velocity of the molybdenum projectile was lower than that of the nickel and copper projectiles. The nickel and copper projectiles had almost the same head velocity. The absolute values of the radial velocity of the molybdenum projectile head was lower than that of the nickel and copper projectiles. However, at $0.75D$ standoff distance, the absolute values of the radial velocity of the molybdenum projectile head became much greater than that of the nickel and copper projectile heads. The projectile formed by BCASC with the molybdenum liner had the highest penetration depth of 61.5 mm, which was 10.0% and 21.3% higher than that generated by the copper and nickel projectiles.

© 2019 Production and hosting by Elsevier B.V. on behalf of China Ordnance Society. This is an open access article under the CC BY-NC-ND license (<http://creativecommons.org/licenses/by-nc-nd/4.0/>).

1. Introduction

Classically shaped charges usually create small-diameter penetration holes, which cannot meet the requirements of large-diameter penetration holes in some special applications, e.g. emergency rescue, a front shaped charge of tandem warhead, and others. Therefore, many researchers have investigated shaped charge technology of creating large-diameter holes in hard targets [1–3]. Leidel [4] designed an annular-jet shaped charge by adding a steel cylinder in charge part. His study showed that the parameters of liner wall thickness variation had an important effect on the formation and penetration of annular-jet shaped charge. König et al. [5] designed a shaped charge which could form an annular EFP. Their study showed that the diameter of the annular EFP formed by the structure was the same to the charge diameter; meanwhile, the length of the EFP was 1/3 times of the charge diameter. By adding a focusing structure on the traditional annular shaped charge, Xu et al. [6] proposed a new type of annular shaped charge. Based on an orthogonal optimization method, they studied

the influence of the liner thickness, cone angle of the focusing structure, the diameter of the nozzle and the thickness of the shell on axial and radial velocity of annular jet. The experimental results showed that the new type of annular shaped charge could form a large-diameter annular hole in steel targets. Grace et al. [7] studied the effect of initiation mode on jet formation of annular shaped charge. Their research indicated that a modest initiation radius could form a tubular jet and peripheral initiation, which caused inward jet flow and thus ultimately resulted in a reconstituted jet.

The liner is the key component of a shaped charge, and its material selection has an important influence on its penetration capability [8–10]. Through theoretical analysis and numerical simulation, Meister et al. [11] designed two kinds of annular shaped charge, i.e., the center-reversed charge and the outer-wall-reversed charge. The experimental results of annular shaped charge with four different liner materials, iron, aluminum, lead and tantalum, showed that the four materials could form an annular jet with certain penetration ability. Wang et al. [12] investigated the effect of liner material (copper, steel, and aluminum) of the shaped charge on jet formation and its penetration capability by experimental and numerical methods. Their study showed that the velocity of copper jet with the strongest penetration capability was higher than that of steel jet but lower than that of aluminum jet. The aluminum jet

* Corresponding author.

E-mail address: wangcheng@bit.edu.cn (C. Wang).

Peer review under responsibility of China Ordnance Society

<https://doi.org/10.1016/j.dt.2019.07.001>

2214-9147/© 2019 Production and hosting by Elsevier B.V. on behalf of China Ordnance Society. This is an open access article under the CC BY-NC-ND license (<http://creativecommons.org/licenses/by-nc-nd/4.0/>).

had the largest velocity with the poorest penetration capability. Zhang et al. [13] studied the influence of liner material on shaped charge penetration created by underwater explosion. As for aluminum, copper and steel liner materials, the jet velocity in the case with the aluminum liner was higher than that for the other two cases. However, the aluminum jet demonstrated the poorest penetration capability. It implies that higher velocity does not always have more serious damage effect.

In this work, we studied the BCASC made of three different liner materials on formation and penetrating into steel targets by experimental and numerical methods. The experimental setup and penetration results of BCASC were presented in section 2, meanwhile the simulation models, material models and parameters were provided in section 3. The validity of the numerical simulation is verified by comparing the numerical simulation results with the test data. Furthermore, the effects of the liner materials on the BCASC formation progress are discussed. Section 4 summarizes some conclusions.

2. BCASC experiments

The bore-center annular shaped charge (BCASC) used in experiments is shown in Fig. 1. The BCASC is mainly composed of a liner, steel shell and composition B explosive (TNT: RDX = 40%: 60%). The D100 mm × L180 mm cylindrical explosive is fully filled in the shell. The thickness of the shell is 2.0 mm. Design and structure of the liners of BCASC is shown in Fig. 2. Three materials of molybdenum, nickel and copper were used for the liners in experiments to study the effect of liner materials on formation and penetration of BCASC. The dimensions of the liners are given in Fig. 2 (b).

The test setup of BCASC penetrating into targets is illustrated in Fig. 3. The material of the targets is 4340 steel. The booster charge with diameter of 25.0 mm was mounted in the end of the BCASC sample. After the booster charge was initiated by a detonator, it would detonate the main charge inside the BCASC sample. The standoff distance between the BCASC sample and the target is 75.0 mm. The targets were made of two stacked cylinders. The diameter of the cylinder target is 250.0 mm and the height is 80.0 mm.

Penetration results of the BCASC with three materials at the standoff distance of $0.75D$ are shown in Fig. 4. All the projectiles were able to generate an annular bullet hole with a rough central conical core in the targets. As listed in Table 1, penetration diameters of annular hole formed by the molybdenum and nickel projectiles are slightly larger than that formed by the copper



Fig. 1. The structure of a bore-center annular shaped charge.

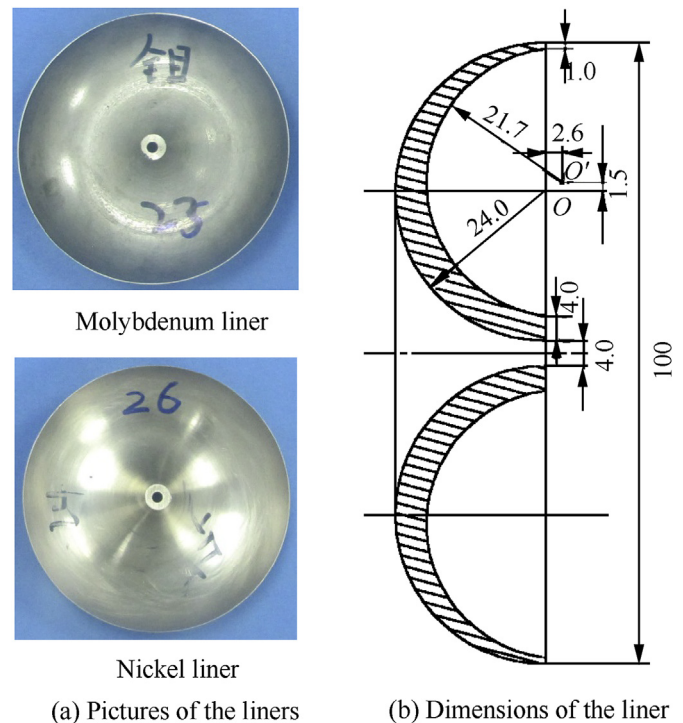


Fig. 2. Design of the liners.

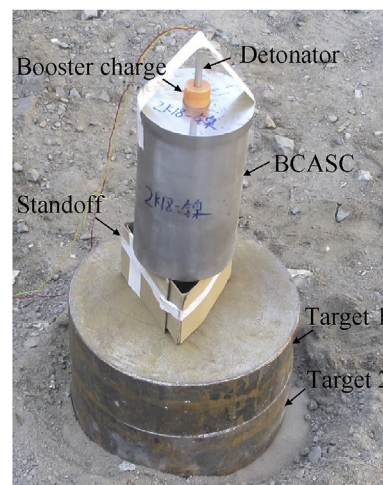


Fig. 3. Test setup of bore-center annular shaped charge penetrating into steel targets.

projectile. The projectile formed by BCASC with the molybdenum liner has the highest penetration depth of 61.5 mm, which is 10.0% and 21.3% higher than that of the copper and nickel projectiles, respectively.

3. Numerical simulation

3.1. Numerical simulation methods

The remapping technology in hydrocode Autodyn was applied to study formation and penetration of BCASC with different liner materials of molybdenum, nickel and copper. Firstly, the formation process of BCASC projectiles was simulated by using Euler solver and 2-dimensional axisymmetric formulation, as shown in Fig. 5.

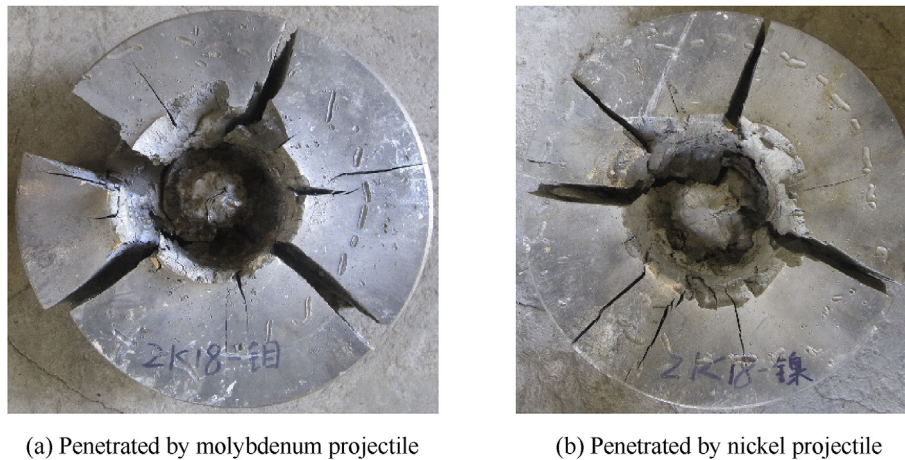


Fig. 4. Penetration results of the BCASC with three materials at 0.75D standoff distance.

Table 1

The measured parameters of the penetrated target.

Penetration results	Molybdenum projectile	Nickel projectile	Copper projectile [1]
Diameter of annular hole /mm	108.5	108.0	105.5
Depth of annular hole /mm	61.5	50.7	55.9

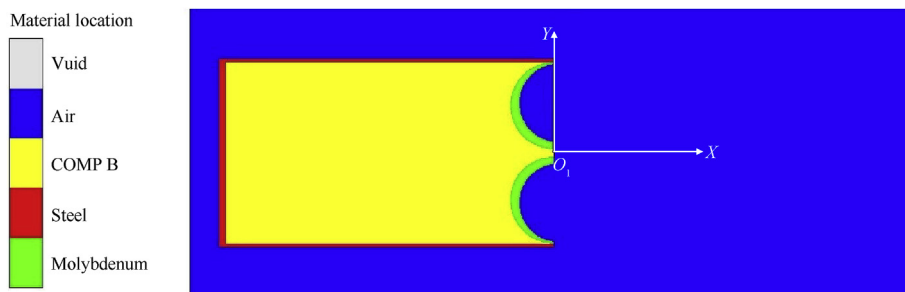


Fig. 5. The simulation model for the formation of BCASC with molybdenum liner.

The coordinate origin is located at the axis of the central hole of the liner with a simulation region of 400 mm × 160 mm and flow-out non-reflection boundaries. Secondly, the simulated results were remapped into the 2D axisymmetric Lagrange mesh to simulate the penetration progress, as shown in Fig. 6. As presented in the previous study [1], to balance reasonable accuracy and computational costs, the size of square mesh for both the Euler and Lagrange was set to be 0.4 mm × 0.4 mm.

The ideal gas model with the below equation of state (EOS) is applied,

$$P_A = (\gamma - 1)\rho_A E_A, \quad (1)$$

where $\rho_A = 1.225 \times 10^{-3} \text{ g/cm}^3$ is the density of air, $\gamma = 1.4$ is the gas constant, $E_A = 206.8 \text{ kJ/m}^3$ is the internal energy per unit mass of air.

The composition B explosive is described by JWL EOS

$$P_B = A_1 \left(1 - \frac{\omega}{R_1 V}\right) e^{-R_1 V} + B_1 \left(1 - \frac{\omega}{R_2 V}\right) e^{-R_2 V} + \frac{\omega E_0}{V}, \quad (2)$$

where P_B is the pressure; $V = 1/\rho_B$ is the specific volume; ρ_B is the density of composition B; E_0 is the specific internal energy per unit mass; A_1, B_1, R_1, R_2 and ω are material constants. The input values

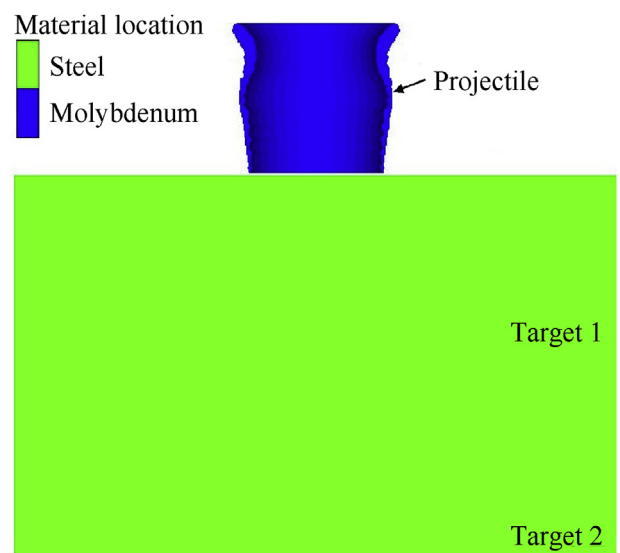


Fig. 6. The simulation model for the penetration of BCASC with molybdenum liner.

are listed in Table 2.

The EOS of the molybdenum, nickel and copper liner is a shock model. And, the strength model of liner is neglected because a liner behaves like a fluid under the extremely large pressure and temperature during collapse [14]. The relationship between material shock velocity (U_S) and particle velocity (u_p), is specified as

$$U_S = C_0 + Su_p, \quad (3)$$

where C_0 is the bulk acoustic sound speed, S is a constant.

Based on the shock Hugoniot, a Mie-Gruneisen form of the EOS is established

$$P = P_H + \Gamma \rho (E - E_H), \quad (4)$$

where it is assumed that $\Gamma \rho = \Gamma_0 \rho_0 = \text{constant}$, $\Gamma = B_0 / (1 + \mu)$ is the Gruneisen Gamma coefficient, B_0 is a constant; $\mu = \rho / \rho_0 - 1$ is the compressibility, ρ_0 is the reference density, P_H is the Hugoniot pressure and E_H is the Hugoniot energy

$$P_H = \frac{\rho_0 C_0^2 \mu (1 + \mu)}{[1 - (S - 1)\mu]^2}, \quad (5)$$

$$E_H = \frac{1}{2} \frac{P_H}{\rho_0} \left(\frac{\mu}{\mu + 1} \right), \quad (6)$$

The EOS of the steel material (shells and targets) is also a shock model and the strength is described by Johnson-Cook model which defines the yield stress Y as

$$Y = (A + B \varepsilon_p^n) (1 + C \lg \dot{\varepsilon}_p^*) (1 - T_H^m), \quad (7)$$

where ε_p is effective plastic strain, $\dot{\varepsilon}_p^* = \dot{\varepsilon}_p / \dot{\varepsilon}_0^*$ with $\dot{\varepsilon}_0^* = 1 \text{ s}^{-1}$ is normalized effective plastic strain rate and $T_H^m = (T - T_{\text{room}}) / (T_{\text{melt}} - T_{\text{room}})$ is the homologous temperature, T_{melt} is the melting temperature, T_{room} is the room temperature, A , B , C , n and m are the material constants. The detailed parameters of the above models are obtained from the Autodyn material library. The input values of the liner, shell and target materials are listed in Table 3.

3.2. Verification of simulation model

At 0.75D standoff distance, the progress of BCASCs with different liner materials penetrating into steel targets are shown in Fig. 7. As shown in simulation results, the penetrated hole walls display a blade shape, which is caused by the radial impact of the projectile. The predicted penetrated diameter and depth of the annular hole are all smaller than the experimental results. The maximum deviation in the diameter and depth of the annular holes between the numerical simulation results and the experimental ones are -9.5% and -8.1% , respectively (see Table 4). The simulation results are consistent well with the test data, indicating that the established simulation model is reliable.

3.3. Discussion

The radial velocities (V_Y) of the projectile are given by the velocity of the elements along a straight path (measuring line) which

Table 2
The input values in the JWL EOS of composition B.

ρ_B (g/cm ³)	E_0 (kJ·m ⁻³)	A_1 (GPa)	B_1 (GPa)	R_1	R_2	ω
1.717	8.50×10^6	524.23	7.678	4.20	1.10	0.34

Table 3
The input parameters for the liner, shell and target materials.

Parameter	Molybdenum	Nickel	Copper	Steel
Equation of state	Shock	Shock	Shock	Shock
Reference density ρ_0 /g·cm ⁻³	10.206	8.874	8.93	7.896
Gruneisen coefficient Γ	1.52	1.93	2.02	2.17
Parameter C_0 /m·s ⁻¹	5124.0	4602.0	3940.0	4596.0
Parameter S	1.233	1.437	1.489	1.49
A /MPa	–	–	–	350.0
B /MPa	–	–	–	275.0
n	–	–	–	0.36
C	–	–	–	0.022
m	–	–	–	1.0
T_{melt} /K	–	–	–	1811.0
T_{room} /K	–	–	–	300.0

passes the center of the projectiles formed by the liner. The distribution of the radial velocities of the projectiles along the path at 0.50D standoff distance is shown in Fig. 8. Along with the direction of the projectile length, the radial velocity of the projectiles formed by the three different liner materials decreases first, then increases and decreases again. Between the tail and the middle part, the difference of the radial velocity of the projectile formed by the three linear materials is negligible. The radial velocity of all the projectile heads is negative, which means, at 0.50D standoff distance, the head of the projectile deflects towards the axis of the charge. Compared to the nickel and copper projectiles, the absolute values of the radial velocity of the head of the molybdenum projectile is obviously lower.

The axial velocities of the projectile mode of the three different liner materials are plotted in Fig. 9. It can be seen that the axial velocities of the projectile gradually increase along the length. Both the nickel and copper projectiles display the same velocity profile, but the axial velocity of the molybdenum projectile is lower than that of the nickel and copper projectiles. However, the numerical simulation and experimental results show that the penetration depth of the molybdenum projectile is higher than that of copper and nickel projectiles. Considering that the density of molybdenum material is much larger than that of copper and nickel, this means that the penetration ability of the projectiles is not only related to the penetration velocity, but also affected by the density of the projectile materials.

The projectiles formed by three liner materials at the moment of impact targets (0.75D) are illustrated in Fig. 10. The velocity (axial velocity V_X' , radial velocity V_Y') and diameter (D_p) of the projectile head and length of the projectile (L_p) formed by the three liner materials are listed in Table 5. It is consistent with the conclusions obtained at 0.50D, for 0.75D standoff distance the V_X' value of molybdenum projectile is less than that of nickel and copper projectiles. However, at 0.75D standoff distance, the radial velocity of the molybdenum projectile head is positive, indicating the head of the projectile turns away from the axis of the charge. Meanwhile, the radial velocity of the head of the molybdenum projectile is much higher than that of the nickel and copper projectile. Both the nickel and copper projectiles display the same configurations with the same D_p and L_p , but the values of D_p and L_p for the molybdenum projectile is slightly larger than that of the nickel and copper projectiles. Although the diameter (D_p) of the projectile head is smaller than that of the charge, the diameter of the penetration hole on the targets is larger than that of the charge because of the radial velocity of the projectiles.

4. Conclusions

The effect of the liner materials, i.e. molybdenum, nickel and

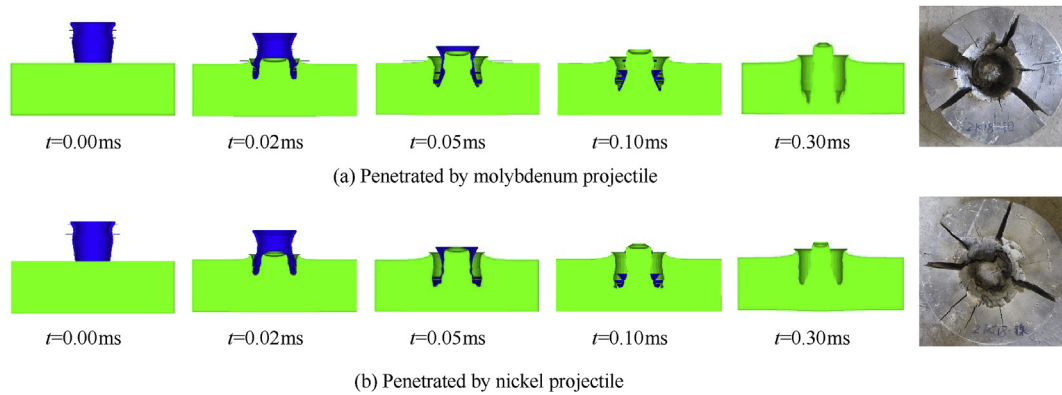


Fig. 7. The progress of BCASCs with different liner materials penetrating into steel targets.

Table 4

The details of numerical and experimental results.

Penetration results	Molybdenum projectile		Nickel projectile		Copper projectile [1]	
	Simulation	Test	Simulation	Test	Simulation	Test
Diameter of annular hole /mm	99.1	108.5	102.9	108.0	104.5	105.5
Depth of annular hole /mm	57.9	61.5	48.1	50.7	51.7	55.9

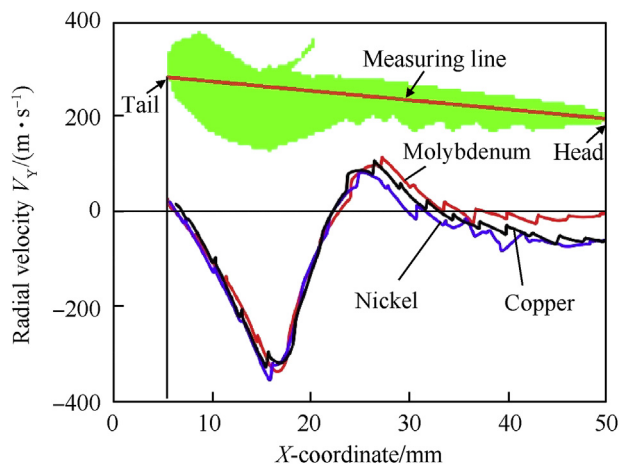


Fig. 8. Distribution of radial velocities of the projectiles along the length at 0.50D standoff.

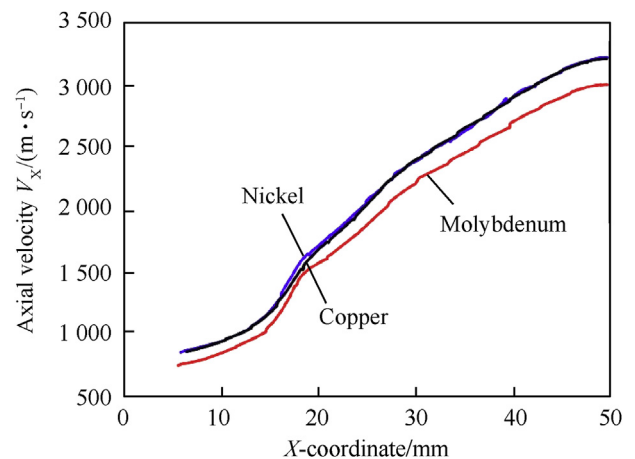


Fig. 9. Distribution of axial velocities of the projectiles along the length at 0.50D standoff.

copper, on the BCASC formation and penetrating into steel targets are investigated by simulation and experiment. The conclusions are drawn as follows:

- 1) The projectile formed by BCASC with molybdenum liner has the highest penetration depth of 61.5 mm, which is 10.0% and 21.3% higher than that of the copper and nickel projectiles, respectively (Table 1 and Fig. 4).
- 2) Along with the direction of the projectile length, the radial velocity of the projectiles formed by the materials of molybdenum, nickel and copper decreases first, then increases and decreases again (Fig. 8).
- 3) At 0.50D standoff distance, the velocity of nickel and copper projectiles head is similar. The absolute values of the radial velocity of the molybdenum projectile head is less than that of the nickel and copper projectile heads (Fig. 8). The axial velocity of

the molybdenum projectile is less than that of the nickel and copper projectiles (Fig. 9).

- 4) At 0.75D standoff distance, the diameter (D_p) of the projectile head and length (L_p) of the projectile formed by BCASC with nickel and copper liners are exactly the same. The values of D_p and L_p of molybdenum projectile is slightly larger than that of the nickel and copper projectiles. The absolute values of the radial velocity of the molybdenum projectile head is much larger than that of the nickel and copper projectile heads (Fig. 10 and Table 5).

The experiments show radial cracking in the targets (Fig. 7), which two-dimensional symmetrical simulation presented in this paper is unable to predict. Three-dimensional simulation work is on-going to investigate how radial cracking affects BCASC penetration into steel targets.

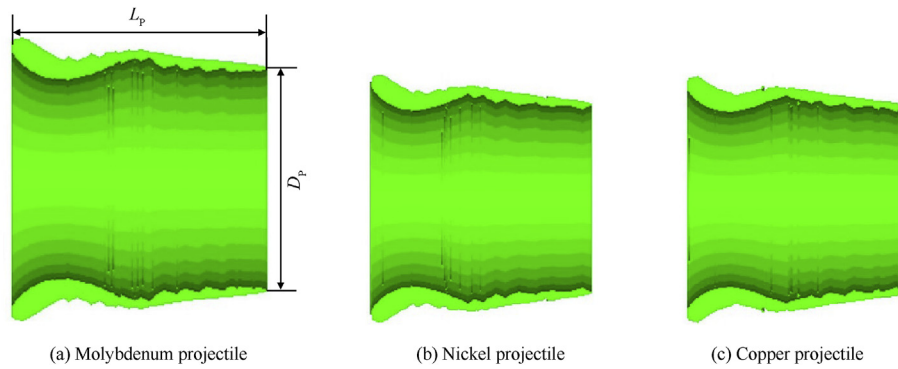


Fig. 10. The projectiles formed by three liner materials at the moment of impact targets (0.75D).

Table 5

The key parameter values of projectiles at the standoff distance of 0.75D.

Type	$V_X' / \text{m} \cdot \text{s}^{-1}$	$V_Y' / \text{m} \cdot \text{s}^{-1}$	D_p / mm	L_p / mm
Molybdenum projectile	2956.3	107.67	56.00	62.33
Nickel projectile	3196.6	-30.72	53.34	61.67
Copper projectile	3170.9	-33.78	53.34	61.67

Acknowledgments

This research is supported by the National Natural Science Foundation of China (No. 11732003), Beijing Natural Science Foundation (No. 8182050), Science Challenge Project (No. TZ2016001) and National Key R&D Program of China (No.2017YFC0804700).

References

- [1] Xu WL, Wang C, Chen DP. Formation of a bore-center annular shaped charge and its penetration into steel targets. *Int J Impact Eng* 2019;127:122–34. <https://doi.org/10.1016/j.ijimpeng.2019.01.008>.
- [2] Rondot FA. Computational parametric study on cookie-cutter projectiles. In: *29th international symposium on ballistics*; 2016.
- [3] Wang C, Huang F, Ning J. Jet formation and penetration mechanism of W typed shaped charge. *Acta Mech Sin* 2009;25(1):107–20. <https://doi.org/10.1007/s10409-008-0212-8>.
- [4] Leidel DJ. A design study of an annular-jet charge for explosive cutting. Drexel University; 1978.
- [5] König PJ, Mostert FJ. The design and performance of annular EFP's. In: *19th international symposium on ballistics*; 2001.
- [6] Xu WL, Wang C, Xu B. Investigation of new type annular shaped charge formation mechanism. *Trans Beijing Inst Technol* 2018;38(6):572–8. <https://doi.org/10.15918/j.tbit1001-0645.2018.06.004>.
- [7] Grace F, Barnard M. Tubular and reconstituted jets using annular shaped charge liners. In: *30th international symposium on ballistics*; 2017.
- [8] Wang ZL, Wang HP, Hou ZH, Xu HY, Li YF. Dynamic consolidation of W-Cu nano-alloy and its performance as liner materials. *Rare Metal Mater Eng* 2014;43(5):1051–5. [https://doi.org/10.1016/S1875-5372\(14\)60099-0](https://doi.org/10.1016/S1875-5372(14)60099-0).
- [9] Guo W, Liu J, Xiao Y, Li SK, Zhao ZY, Cao J. Comparison of penetration performance and penetration mechanism of w-cu shaped charge liner against three kinds of target: pure copper, carbon steel and Ti-6Al-4V alloy. *Int J Refract Met Hard Mater* 2016;60:147–53. <https://doi.org/10.1016/j.ijrmhm.2016.07.015>.
- [10] Xiao JG, Zhang XP, Guo ZX, Wang HF. Enhanced damage effects of multi-layered concrete target produced by reactive materials liner. *Propellants, Explos Pyrotech* 2018;43(9):955–61. <https://doi.org/10.1002/prep.201800105>.
- [11] Meister J, Häller F. Experimental and numerical studies of annular projectile charges. In: *19th international symposium on ballistics*; 2001.
- [12] Wang C, Ding J, Zhao H. Numerical simulation on jet formation of shaped charge with different liner materials. *Def Sci J* 2015;65(4):279–86. <https://doi.org/10.14429/dsj.65.8648>.
- [13] Zhang ZF, Wang LK, Ming F, Silberschmidt VV, Chen HL. Application of Smoothed Particle Hydrodynamics in analysis of shaped-charge jet penetration caused by underwater explosion. *Ocean Eng* 2017;145:177–87. <https://doi.org/10.1016/j.oceaneng.2017.08.057>.
- [14] Elshenawy T, Elbeih A, Li QM. Influence of target strength on the penetration depth of shaped charge jets into RHA targets. *Int J Mech Sci* 2018;136:234–42. <https://doi.org/10.1016/j.ijmecsci.2017.12.041>.